physics

MDPI

Article

Large Angular Momentum States in a Graphene Film

Pietro Paolo Corso, Dario Cricchio and Emilio Fiordilino *

Dipartimento di Fisica e Chimica-Emilio Segré, Università degli Studi di Palermo, Via Archirafi 36, 90123 Palermo, Italy; pietropaolo.corso@unipa.it (P.P.C.); dario.cricchio@unipa.it (D.C.)
* Correspondence: emilio.fiordilino@unipa.it

Abstract: At energy lower than 2 eV, the dispersion law of the electrons in a graphene sheet presents a linear dependence of the energy on the kinetic momentum, which is typical of photons and permits the description of the electrons as massless particles by means of the Dirac equation and the study of massless particles acted upon by forces. We analytically solve the Dirac equation of an electron in a graphene disk with radius of 10,000 atomic units pierced by a magnetic field and find the eigenenergies and eigenstates of the particles for spin up and down. The magnetic field ranges within three orders of magnitude and is found to confine the electron in the disk. States with a relatively large total angular momentum exist and can be considered in a vorticose condition; these states are seen to peak at different distances from the disk centre and can be used to store few bit of information.

Keywords: graphene; Dirac electron; Dirac equation; graphene eigenstates in a magnetic field

1. Introduction

The modern technological state of the art permits the fabrication of materials endowed with new and astounding properties, able to disclose physical effects not seen before. Among these new materials, reduced-dimensionality nano and mesoscopic objects are gaining increasing interest in fundamental as well as applied research. They are characterised by the feature that at least one of their spatial sizes is much smaller that the others; the energy required to populate the levels pertaining to the relatively small dimension is much larger than that required for the other dimensions so that the small dimension can be disregarded in the mathematical description of the physical object; therefore, the system can be safely studied by means of a lower number of degrees of freedom. The conceptual interest in the possibility of experimentally exploring systems with a smaller number of degrees of freedom is evident but the technological repercussions have been shown to be of great importance too.

Among these new physical objects, one can include quantum dots, nano and meso rings and nano tubes, all deserving special consideration. Quantum dots are small clumps of semiconductor, confined within a convenient substrate and possessing a spectrum of discrete energy levels that can be designed almost at will to fulfil particular requirements and for this characteristics are pictorially referred to as artificial atoms; they can be seen as zero dimensionality systems. Particular mention must be devoted to the rich variety of allotropes of the carbon atom as some of them can be used to produce reduced dimensionality systems. For example, C_{60} fullerene is a spherical arrangement of carbon atoms, situated at the corners of hexagons and pentagons, that can be described as a zero- or a two-dimensional object.

On the other hand, graphene is a flat monolayer of carbon atoms placed at the corners of a pattern of hexagons of side $L \cong 2.7a_0$, with a_0 the Bohr radius, and resembling a honeycomb; it is one of the most interesting materials for fundamental and applied research. At energy lower than 2 eV, owing to the particular symmetry of the lattice, the

check for updates

Citation: Corso, P.P.; Cricchio, D.; Fiordilino, E. Large Angular Momentum States in a Graphene Film. *Physics* **2024**, *6*, 317–333. https://doi.org/10.3390/physics6010021

Received: 10 November 2023
Revised: 13 January 2024
Accepted: 16 January 2024
Published: 1 March 2024

valence and conduction bands slightly overlap [1,2], producing a linear dependence of the electron energy, E, upon the modulus of the kinetic momentum, π:

$$E = v_F \pi, \tag{1}$$

where $v_F = u_F c$ is the Fermi speed of the electrons in the layer, c the speed of the light and $u_F \cong 1/300$ a dimensionless numerical constant. The linear dispersion is typical of the photon, which allows the description of the charge carriers as massless, free fermions moving with speed v_F [1,3,4] and gives the opportunity of studying zero-mass charges which, nevertheless, can be acted upon by electromagnetic forces; in this way, a new phenomenon with no classical counterpart is open to investigation. Even if $v_F < v_{1s}$ with $v_{1s} \cong c/137$, the average electron speed in the hydrogen ground state, one can see that the description of the charge carriers by using the Schrödinger equation is impossible and the Dirac equation must be used after the substitution $c \to v_F$.

In the Dirac electron theory, the dual presence of a positive–negative energy solution, or electron–positron pair, is inherent and the Klein paradox makes the confinement of relativistic fermions by means of a repulsive potential barrier larger than $2mc^2$ quite complicated, it would act as a chasm for the negative energy solution of the Dirac equation. Actually, in the presence of a large enough barrier, the positive energy solution of the Dirac equation disappears from the classical permitted zone of the space and makes a transition into the negative energy state solution by appearing in the classical forbidden zone of the space [5].

In graphene, the condition of massless fermions is valid at low energy and for an infinite sheet, although the latter condition can be safely overcome by using quite large fragments of film. In spite of the finding that the formalism is quite similar, in graphene, actually, there is no room for the electron–positron interpretation of the positive and negative energy solution and the two solutions are to be interpreted as states in the valence and conduction bands. Nevertheless, the similarity of the theory makes a phenomenon similar to the Klein paradox present also in graphene, where the electron, moving in the conduction band of the film, in impinging upon a potential barrier, appears in the region of the step in the valence band [6]. Thus, several confinement schemes, based on magnetised pieces of graphene [2,7–11], or on the presence of electric and magnetic fields [12–16], have been devised.

Graphene is the strongest known material [17] and endowed with a quite a large charge mobility [18]: because of these and other properties, it is one of the most promising materials for applicative research in Medicine, Chemistry, Informatics and Physics. Among the many applications, we mention the use in efficient solar cells [19], which could help the increasing demand for electrical energy with a quite low environmental impact, and as a frequency multiplier of laser light in the well-known high harmonic generation [20–22]. Considering graphene, most interesting is the finding that, by suitable manipulation, it is possible to obtain, from the basic honeycomb structure, different systems possessing different dimensionality. Actually, graphene sheets can be rolled to form quite long and slender cylinders, dubbed nano tubes, and cones with lengths several orders of magnitude larger than the radius and, by cutting from tubes, nano rings can also be fabricated with unidimensional properties. Also by cutting a graphene sheet, two dimensional annuli and disks can be prepared. Another fascinating development is the realisation of elaborate three-dimensional graphene structures inspired by origami [23–25].

Today, computer technology prompts the design and fabrication of meso- and nano-sized electronic components for information storage and as the fastest logic circuital elements [26–29]. However, saturation in the performance of traditional silicon devices is presently observed so that the quest for new material is active; in this context, graphene and other carbon allotropes, such as C_{60}, fullerene and carbon tubes, are natural candidates for their quick response to external fields and high-frequency operation. Therefore, the comprehension of the behaviour of carbon-based material as C_{60} molecules, quantum rings and annuli acted upon by static or dynamic electromagnetic fields is of paramount

importance. Far from being of hindrance to the theoretical approach, the quite large size of these molecules may create symmetries which, judiciously exploited, produce deep simplification in the theoretical approach to the problem and often leads to analytical solutions or crucial insight into the physics of the problem [30].

This paper deals with a disk of graphene of radius ρ_1 = 10,000 a_0 crossed by a static magnetic field B_0. The quite large radius ρ_1 of the disk makes the dispersion law in Equation (1) and the massless condition of the charge carriers suitable approximations. Moreover, the large size makes the inevitable irregularity and roughness at the disk border insignificant as it is well known that armchair or zigzag edges give different spectra in graphene ribbons [1,31]. We analytically solve the Dirac equation for the charge carriers by finding the eigenstates and relative energy as a function of the magnetic field and numerically evaluate them. As a result, we find that the magnetic field has a strong confinement action on the electron and that relatively large orbital angular momentum states are supported by the disk. These states are confined in different regions and might be used to store several bits of information; since large angular momenta states of Bose–Einstein condensate, vortices, confined in spherical surfaces and rings, are currently actively investigated [32–35], graphene disks can be suitable candidates for studying vortices states with simple enough equipment.

2. Theory

Several equivalent representations of the Dirac equation can be given that are related by a unitary transformation. The commonest forms are the standard representation that is mostly useful in weak relativistic approximations and the chiral representation which is mostly useful in ultrarelativistic regimes, when the energy of the particle is much larger than the rest energy. For reasons that will soon be clear, in what follows, the chiral representation is used. Thus, the Dirac equation for a fermion of charge q and mass m_q in the presence of a magnetic field in the chiral representation is

$$\begin{cases} \left[-\vec{\sigma}\cdot\left(\underset{\sim}{\vec{p}}-\frac{q}{c}\vec{A}\right)-i\hbar\partial_0\right]\dot{\Psi}^{(L)}=-m_q c\dot{\Psi}^{(R)}, \\ \left[\vec{\sigma}\cdot\left(\underset{\sim}{\vec{p}}-\frac{q}{c}\vec{A}\right)-i\hbar\partial_0\right]\dot{\Psi}^{(R)}=-m_q c\dot{\Psi}^{(L)}, \end{cases} \tag{2}$$

where $\vec{\sigma}=(\sigma^1,\sigma^2,\sigma^3)$ is the triplet of the Pauli matrices, $\underset{\sim}{\vec{p}}=-i\hbar\vec{\nabla}$ the canonical momentum operator (denoted by a tilde below the symbol), $\hbar$ is the reduced Planck constant, $\vec{A}$ the vector potential, $\partial_0\equiv\partial/\partial ct$, t denotes the time, and $\dot{\Psi}^{(L)}$ and $\dot{\Psi}^{(R)}$ are the time-dependent left and right two-component Weyl spinors (denoted by a dot below the symbol), respectivly, forming the four component Dirac spinor in the chiral representation. $\dot{\Psi}^{(L)}$ and $\dot{\Psi}^{(R)}$ depict the positive and negative energy states of the fermion. Care must be taken in handling $\vec{\sigma}$ because, in spite of the look, under a spatial rotation it does not transform like a vector; it must be regarded as a convenient notational device that accounts for the mixing of the spinor components. From Equation (2), one sees that the mass couples the left and right spinors. In our model, however, the mass and the related rest energy are zero so that the equations for the two components uncouple:

$$\begin{cases} \left[-\vec{\sigma}\cdot\left(\underset{\sim}{\vec{p}}-\frac{q}{c}\vec{A}\right)-i\hbar\partial_0\right]\dot{\Psi}^{(L)}=\dot{0}, \\ \left[\vec{\sigma}\cdot\left(\underset{\sim}{\vec{p}}-\frac{q}{c}\vec{A}\right)-i\hbar\partial_0\right]\dot{\Psi}^{(R)}=\dot{0}, \end{cases} \tag{3}$$

and differ only for a sign; thus, the positive and negative energy solutions behave independently. For the sake of brevity, only the first equation, with the superscript (L) dropped out, is studied here. For the Dirac charge (after the default substitution $c\rightarrow cu_F$), $\dot{\Psi}$ assumes the form of a time-dependent Schrödinger equation,

$$i\hbar\partial_t\dot{\Psi}=-cu_F\vec{\sigma}\cdot\left(\underset{\sim}{\vec{p}}-\frac{q}{c}\vec{A}\right)\dot{\Psi}, \tag{4}$$

with the Hamiltonian,

$$\underset{\sim}{H} = -cu_F\vec{\sigma}\cdot\left(\underset{\sim}{\vec{p}} - \frac{q}{c}\vec{A}\right). \tag{5}$$

One recognises in the operator $\underset{\sim}{\vec{\pi}} \equiv \underset{\sim}{\vec{p}} - (q\vec{A}/c)$ the kinetic momentum operator. The Hamiltonian is related to the helicity operator. As mentioned in Section 1, in general, for studying the properties of ultrarelativistic electrons, Equation (3) is used approximately. In the case of graphene, for the vanishing of the mass, this use is necessary and offers the opportunity to investigate relativistic effects without making use of large accelerators.

2.1. Total Angular Momentum

In this paper, we consider that the static magnetic field

$$\vec{B}_0 = B_0(0,0,1), \tag{6}$$

generated by the vector potential,

$$\vec{A}_0 = \frac{1}{2}\vec{B}_0\times\vec{r} = \frac{B_0}{2}(-x^2, x^1, 0), \tag{7}$$

pierces a disk of radius ρ_1 whose centre $\boldsymbol{r}_c$ lays at the origin of the (x^1x^2)-plane, $\boldsymbol{r}_c = (0,0)$. The particular geometry of the system suggests that the third component of the total angular momentum is a constant and that to seek common eigenstates of the Hamiltonian and this component of the angular momentum operators is convenient. The calculations to find the expressions for the operators and to obtain their equation of motion require quite an amount of algebra and may be rather long. In what follows, we confine ourselves to outlining the significant steps and the interested reader may find details in [5,36].

Thus, after long but straightforward use of commutator algebra, the equation

$$\frac{d\underset{\sim}{\vec{J}}}{dt} = \frac{qu_F}{2}\vec{B}_0\times(\vec{r}\times\vec{\sigma}) \tag{8}$$

for the total angular momentum $\underset{\sim}{\vec{J}}$ (in units of $\hbar$) is arrived at. One can see that the time derivative of $\underset{\sim}{\vec{J}}$ is orthogonal to the magnetic field, so that the component of the total angular momentum along the magnetic field,

$$\underset{\sim}{J^3} \equiv -i\partial_\varphi + \frac{1}{2}\sigma^3, \tag{9}$$

is constant and admits common eigenstates with the Hamiltonian. Here, φ is the polar angle. Moreover, as discussed in Section 1, in materials with reduced dimensionality, the active electron can be described as confined on the disk to be considered as a two-dimensional object.

We begin by considering the eigenstates of the angular momentum. In circular variables, the eigenvalue equation is $\underset{\sim}{J^3}\dot{\psi}(\rho,\varphi) = j_3\dot{\psi}(\rho,\varphi)$, with ρ the radial variable and j_3 the angular momentum eigenvalue. The two components of the time-independent spinor $\dot{\psi}(\rho,\varphi)$ correspond to the two projections of the angular momentum along the magnetic field. After splitting $\dot{\psi}(\rho,\varphi)$ into its components by setting

$$\dot{\psi}(\rho,\varphi) = \begin{pmatrix}\Phi_1(\varphi)R_1(\rho)\\ \Phi_2(\varphi)R_2(\rho)\end{pmatrix} \tag{10}$$

and sustituting into Equation (9), one obtains

$$\left(-i\partial_\varphi + \frac{1}{2}\sigma^3\right)\begin{pmatrix}\Phi_1(\varphi)R_1(\rho)\\ \Phi_2(\varphi)R_2(\rho)\end{pmatrix} = j_3\begin{pmatrix}\Phi_1R_1\\ \Phi_2R_2\end{pmatrix}, \tag{11}$$

equivalent to the two coupled differential equations for the angular part:

$$\begin{cases} \dfrac{d\Phi_1}{d\varphi} = i\left(j_3 - \dfrac{1}{2}\right)\Phi_1\,, \\ \dfrac{d\Phi_2}{d\varphi} = i\left(j_3 + \dfrac{1}{2}\right)\Phi_2\,, \end{cases} \tag{12}$$

with the solution

$$\begin{cases} \Phi_1(\varphi) = \dfrac{\mathrm{e}^{im\varphi}}{\sqrt{2\pi}}\,, \\ \Phi_2(\varphi) = \dfrac{\mathrm{e}^{i(m+1)\varphi}}{\sqrt{2\pi}}\,, \end{cases} \tag{13}$$

where m is the quantum number of the orbital angular momentum,

$$m = j_3 - \frac{1}{2} = \ldots, -2, -1, 0, 1, 2, \ldots\,. \tag{14}$$

Let us stress that j_3 and not m is the conserved quantity. Actually, it is a straightforward task to check, by direct calculations, that $\psi(\rho, \varphi)$ is not eigenstate of ϖ^3.

In order to obtain the form of the equation for the radial parts, many tedious steps are required [36]; the result is

$$\underset{\sim}{H}\psi_m = i\hbar c u_F \left[\frac{\mathrm{e}^{im\varphi}}{\sqrt{2\pi}}\begin{pmatrix} R_2' \\ \mathrm{e}^{i\varphi}R_1' \end{pmatrix} + \frac{1}{\rho}\frac{\mathrm{e}^{im\varphi}}{\sqrt{2\pi}}\begin{pmatrix} (m+1)R_2 \\ -m\mathrm{e}^{i\varphi}R_1 \end{pmatrix}\right] + \frac{qu_F B}{2}\rho\frac{\mathrm{e}^{im\varphi}}{\sqrt{2\pi}}\begin{pmatrix} -iR_2 \\ i\mathrm{e}^{i\varphi}R_1 \end{pmatrix} \tag{15}$$

with the prime denoting differentiation with respect to ρ. Surely, the subscript m had to be added to the wave function. Actually, notational rigorousness would require that the same index should flag the radial wave functions R_1 and R_2 but symbolism would become heavy and cumbersome and requires refraining from full coherence.

The eigenenergy equation is

$$\begin{cases} iu_F\left[\hbar c\left(\dfrac{d}{d\rho} + \dfrac{m+1}{\rho}\right) - \dfrac{qB_0}{2}\rho\right]R_2 = ER_1\,, \\ iu_F\left[\hbar c\left(\dfrac{d}{d\rho} - \dfrac{m}{\rho}\right) + \dfrac{qB_0}{2}\rho\right]R_1 = ER_2\,, \end{cases} \tag{16}$$

where the energy E, common to both the spin components, and the radial functions $R_1(\rho)$ and $R_2(\rho)$ must be found simultaneously. The two coupled first-order equations are not of immediate solution and substitution of $R_2(\rho)$ from the second into the first equation is convenient. The procedure leads to a second-order differential equation and is similar to the one that leads from the first-order Maxwell equation to the second-order differential equation for the potentials. The result is

$$\frac{d^2R_1}{d\rho^2} + \frac{1}{\rho}\frac{dR_1}{d\rho} + \left[\frac{E^2}{\hbar^2(u_Fc)^2} + \frac{qB_0(m+1)}{\hbar c} - \frac{q^2B_0^2}{4\hbar^2c^2}\rho^2 - \frac{m^2}{\rho^2}\right]R_1 = 0. \tag{17}$$

To work with a dimensionless variable, it is convenient to define

$$x = \rho^2/\lambda^2, \tag{18}$$

where

$$\lambda^2 \equiv \frac{2\hbar c}{|q|B_0} \tag{19}$$

has the dimension of length square. Thus, the parameter λ introduces in the problem a length scale, inversely proportional to $\sqrt{B_0}$, and measures the confinement range induced by the field. In terms of the new variable (18), Equation (17) for R_1 thus reads

$$x^2\frac{d^2R_1}{dx^2}+x\frac{dR_1}{dx}+\left(-\frac{x^2}{4}+\frac{\omega^2}{4}x-\frac{m^2}{4}\right)R_1=0 \tag{20}$$

where

$$\omega^2=\frac{2E^2}{\hbar u_F^2 c|q|B_0}+2\eta(m+1) \tag{21}$$

with $\eta=|q|/q$ the sign of the charge.

The substitution,

$$R_1(x)=\mathrm{e}^{-x/2}x^{|m|/2}f(x), \tag{22}$$

leads to the known confluent hypergeometric equation (CHE):

$$xf''+(|m|+1-x)f'-\left(\frac{|m|+1}{2}-\frac{\omega^2}{4}\right)f=0. \tag{23}$$

The standard form for the CHE is

$$zw''+(b-z)w'-aw=0 \tag{24}$$

admitting two independent solutions, $M(a,b,z)$ and $U(a,b,z)$, which can be written as infinite series. The expression of $M(a,b,z)$

$$M(a,b,z)=1+\frac{a}{b}\frac{z}{1!}+\frac{a(a+1)}{b(b+1)}\frac{z^2}{2!}+\ldots \tag{25}$$

gives few problems. The expansion of $U(a,b,z)$

$$U(a,b,z)=\frac{\pi}{\sin\pi b}\left[\frac{M(a,b,z)}{\Gamma(1+a-b)\Gamma(b)}-z^{1-b}\frac{M(1+a-b,2-b,z)}{\Gamma(a)\Gamma(2-b)}\right] \tag{26}$$

which is well behaved (as a limit) for integer b [37], is not straightforwardly numerically approached because of the presence of the $\sin\pi b$ and of the Γ function of negative integer that can lead to divergences, the latter are quite difficult to handle. Indeed, the one of interest here is located in the hard subset of the problem because, in our model, b is always an integer.

Looking at the expression (23), one determines the parameters of the confluent hypargeometric functions (CHFs) in terms of the relevant physical quantities:

$$a=\frac{|m|+1}{2}-\frac{E^2}{2\hbar u_F^2 c|q|B_0}-2\eta(m+1) \tag{27}$$

$$b=|m|+1. \tag{28}$$

Again, we stress that the feature that b is a positive integer be carefully addressed during the numerical evaluation of $U(a,b,z)$.

To summarize, the radial function $R_1(x)$ has two independent solutions:

$$R_{1;1}(\rho)=\mathrm{e}^{-\frac{\rho^2}{2\lambda^2}}\left(\frac{\rho}{\lambda}\right)^{|m|}M\left(a,b,\frac{\rho^2}{\lambda^2}\right) \tag{29}$$

and

$$R_{1;2}(\rho)=\mathrm{e}^{-\frac{\rho^2}{2\lambda^2}}\left(\frac{\rho}{\lambda}\right)^{|m|}U\left(a,b,\frac{\rho^2}{\lambda^2}\right) \tag{30}$$

which correspond to the spin-up component of the spinor.

The analytic evaluation of the radial functions of the spin down is possible starting from these expressions but requires a lot of algebra of the CHF and is detailed in Appendix A. The final result is

$$R_{2;1}(\rho) = \frac{iu_F}{E}\mathrm{e}^{-\frac{\rho^2}{2\lambda^2}}\frac{\rho^{|m|-1}}{\lambda^{|m|}}\left\{\left[\hbar c\left((\eta-1)\frac{\rho^2}{\lambda^2}+|m|-m\right)\right]M\left(a,b,\frac{\rho^2}{\lambda^2}\right) + 2\frac{a}{b}\frac{\rho^2}{\lambda^2}M\left(a+1,b+1,\frac{\rho^2}{\lambda^2}\right)\right\} \quad (31)$$

and

$$R_{2;2}(\rho) = \frac{iu_F}{E}\mathrm{e}^{-\frac{\rho^2}{2\lambda^2}}\frac{\rho^{|m|-1}}{\lambda^{|m|}}\left\{\left[\hbar c\left((\eta-1)\frac{\rho^2}{\lambda^2}+|m|-m\right)\right]U\left(a,b,\frac{\rho^2}{\lambda^2}\right) - 2a\frac{\rho^2}{\lambda^2}U\left(a+1,b+1,\frac{\rho^2}{\lambda^2}\right)\right\}. \quad (32)$$

In $R_{2;1}(\rho)$ and $R_{2;2}(\rho)$, the presence of the term $|m|-m$ is rather interesting as it acts in different ways for positive and negative m. Actually, the study of a positive charge ($\eta = 1$) and positive m would flow into a tremendous simplification of the formulas as one piece of the wave functions would vanish. The general radial wave functions are given by a linear combination of these functions:

$$\begin{cases} R_1(\rho) = \mu R_{1;1}(\rho) + \nu R_{1;2}(\rho), \\ R_2(\rho) = \mu R_{2;1}(\rho) + \nu R_{2;2}(\rho), \end{cases} \quad (33)$$

where μ and ν are constants to be found from the boundary conditions and normalisation condition.

For a fixed value of m, one observes that a can be maintained constant by keeping $B_0 \propto E^2$ and this would give the dependence of the eigenenergies from the magnetic field; this is, nevertheless, of little use as λ is dependent upon B_0.

2.2. Boundary Conditions

In this paper, we consider a disk with a sharp edge. Actually, no real fragment of graphene can have a sharp border and studies of graphene ribbons have shown that the form of the edges is relevant for the determination of the states of the charges [31]. Again, this approximation can be made weak by considering a disk with a large enough radius ρ_1 so that roughness is not relevant.

The fulfilment of the boundary conditions permits the determination of the eigenstates and eigenenergies (the eigenvalues of the total angular momentum were already found in Equation (14))

$$R_1(\rho_1) = R_2(\rho_1) = 0. \quad (34)$$

To avoid long final expressions, let us introduce the constants

$$M_1(\rho_1) \equiv M\left(a,b,\frac{\rho_1^2}{\lambda^2}\right), \quad U_1(\rho_1) \equiv U\left(a,b,\frac{\rho_1^2}{\lambda^2}\right), \quad (35)$$

$$M_2(\rho_1) \equiv M\left(a+1,b+1,\frac{\rho_1^2}{\lambda^2}\right), \quad U_2(\rho_1) \equiv U\left(a+1,b+1,\frac{\rho_1^2}{\lambda^2}\right), \quad (36)$$

$$C(\rho_1) \equiv \hbar c\left[(\eta-1)\frac{\rho_1^2}{\lambda^2}+|m|-m\right]M_1(\rho_1) + 2\frac{a}{b}\frac{\rho_1^2}{\lambda^2}M_2(\rho_1) \quad (37)$$

and

$$D(\rho_1) \equiv \hbar c \left[(\eta - 1)\frac{\rho_1^2}{\lambda^2} + |m| - m \right] U_1(\rho_1) - 2a\frac{\rho_1^2}{\lambda^2} U_2(\rho_1), \tag{38}$$

so that the boundary conditions assume the form of a two-variable, homogeneous linear algebraic equation:

$$\begin{cases} \mu M_1(\rho_1) + \nu U_1(\rho_1) = 0, \\ \mu C(\rho_1) + \nu D(\rho_1) = 0, \end{cases} \tag{39}$$

where the unknown coefficients μ and ν may be determined only if the determinant of the coefficients vanishes:

$$M_1(\rho_1)D(\rho_1) - U_1(\rho_1)C(\rho_1) = 0. \tag{40}$$

Remembering that E is present in the expression of a, one can see that the values of E that fulfil the condition in Equation (40) are the allowed values of the energies. The problem is therefore fully analytically solved:

$$\nu = -\frac{M_1(\rho_1)}{U_1(\rho_1)}\mu\,, \tag{41}$$

$$\begin{cases} R_1(\rho) = \mu \left[R_{1;1}(\rho) - \dfrac{M_1(\rho_1)}{U_1(\rho_1)} R_{1;2}(\rho) \right], \\ R_2(\rho) = \mu \left[R_{2;1}(\rho) - - \dfrac{M_1(\rho_1)}{U_1(\rho_1)} R_{2;2}(\rho) \right]. \end{cases} \tag{42}$$

The value of μ is found by the normalisation of the wave functions:

$$\int_0^{+\infty} |R_\ell(\rho)|^2 \rho d\rho = 1, \quad \ell = 1, 2. \tag{43}$$

2.3. Helicity

As it quite straightforward to see by direct calculation, the Hamiltonian eigenfunctions are not eigenstates of ϖ^1 and ϖ^2 and the spin projections on the (x^1x^2)-are not individually constant but the helicity is constant. The helicity operator $\underset{\sim}{\mathfrak{h}}$ can be defined as

$$\underset{\sim}{\mathfrak{h}} \equiv \frac{\vec{\varpi} \cdot \vec{\underset{\sim}{\pi}}}{2E} = -\frac{\underset{\sim}{H}}{2cu_F E} \tag{44}$$

so that the helicity evaluated on the energy eigenstates is constant. Generally, the helicity gives the projection of the spin on the kinetic momentum. In our model, both $\vec{\pi}$ and $\vec{A}_0$ lie on the (x^1x^2)-plane (see Equation (7)), so only the projection of the spin in this plane is relevant. The finding that in the present model of disk, the Hamiltonian $\underset{\sim}{H}$ shares the eigenstates with the helicity is helpful feature as helicity is the only degree of freedom for massless particles. One can expect that, the orbital angular momentum is associated with a rotation around an axis; the fact that here the eigenstates of the energy are not eigenstates of $\underset{\sim}{L}^3$ and that m is not a proper quantum number, hinders the possibility of giving a transparent meaning to vortex states.

3. Results and Conclusions

In what follows, we adopt atomic units (au) ($|e| = \hbar = m_e = 1$); thus, the Bohr radius a_0 is the unit of length, the unit of energy is 27.21 eV and $B = 1$ au $= 2.35 \cdot 10^5$ T. The radius of the disk is ρ_1 = 10,000 a_0, the large value ensuring that the electron can be treated as massless; the magnetic field is taken in the interval $B_0 \in [10^{-7}, 10^{-4}]$ au. To find the values of E that solve Equation (40) is a complicated enough task because, as comes from their power expansion, the CHFs are especially sensitive to the value of their parameters; nevertheless, we have checked our results against numerical precision and found no mistakes.

From the expression of the parameters and of the wave functions, we observe that the energy always appears through the ratio E/u_F and therefore we use this ratio as the relevant parameter and, generally, call it energy. Through the parameter a in Equation (27), the energy enters the equations with the ratio E^2/B_0, showing an intrinsic weak dependence of the eigenvalues upon $\sqrt{B_0}$. The parameters of the CHF are quite sensitive to the value of the magnetic field B_0 and this dependence is rather crucial at low enough B_0. Thus, actually, the results are stabler and more reliable at large enough B_0. For any value of m, there are several eigenstates fulfilling the boundary conditions and these eiegenstates are numbered with the integer n; thus, to label the eigenenergies and, consequently the relative eigenstates, the second subscript n must be introduced as $E_{m;n}$. For $m \geq 0$, n counts the number of nodes of the eigenstates between the centre and the disk edge. For $m < 0$, such an appealing correspondence is not realised and the number of nodes can be $n + 1$. We have performed numerical calculations to determine the eigenvalues and eigenstates of the Dirac electron in the disk for different values of B_0, m and n; in all the calculations, we have considered a negative charge: $\eta = q/|q| = -1$.

Figure 1A shows the eigenengies of the Dirac electron versus the magnetic field for $n = 0$ and for different values of the orbital angular momentum, m. For non-negative m, $E_{m,n}$ increases with B_0 and m and observe the mentioned weak dependence of $E_{m,n}$ on B_0. Relegated in the lower left corner of the figure, the curve for $m = -5$ pops up with its considerably small energy and decreasing behaviour. Figure 1B shows the eigenenergies of the electron versus n at $B_0 = 5.0 \times 10^{-5}$ au for different value of the orbital angular momentum. The eigenvalues increase almost linearly with n and can be extrapolated with confidence.

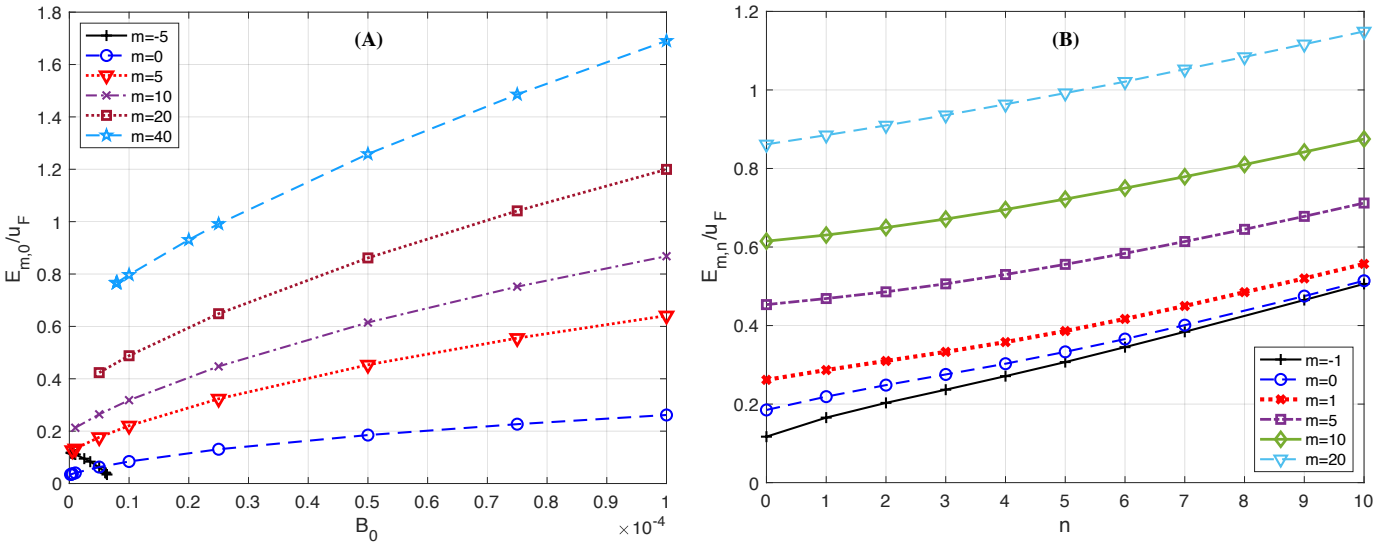

Figure 1. (**A**) Eigenenergies (in atomic units, au) versus the magnetic field (in au) for different values of the orbital angular momentum, m, and $n = 0$. The energy of the states increases with B_0 because the parameter a in the CHFs depends on the the ratio E^2/B_0 (see Equation (27)). (**B**) Eigenenergies versus n for different values of m and the magnetic field $B_0 = 5 \times 10^{-5}$ au. Now the energy of the states increases with n because the area where the charge can be found is decreased by the presence of n nodes in the eigenstates.

The meaning of the integer n can be understood from Figure 2 where we show few eigenstates at $m = 0$ and different values of n. Figure 2A displays the case of spin up. The states peak always at the centre of the disk and present n nodes (the node at the disk edge is there by construction). The case for the spin down is shown in panel Figure 2B. Now, the states have a node at the origin and present again n nodes between border and edge. The presence of the nodes gives an expected explanation of the growth in the energy as

shown in Figure 1B since the nodes have the effect of decreasing the available area of the disk, thus confining the charge in a smaller area.

Actually, the description is not so clear-cut for negative m. In Figure 3, the case for $m = -1$ is shown. For spin up, n again gives the number of nodes between the centre and edge of the disk. In the spin-down case, on the other hand, the eigenstates show $n + 1$ nodes. To stress is that states with the same n (in Figure 3A,B) correspond to the same eigenvalue.

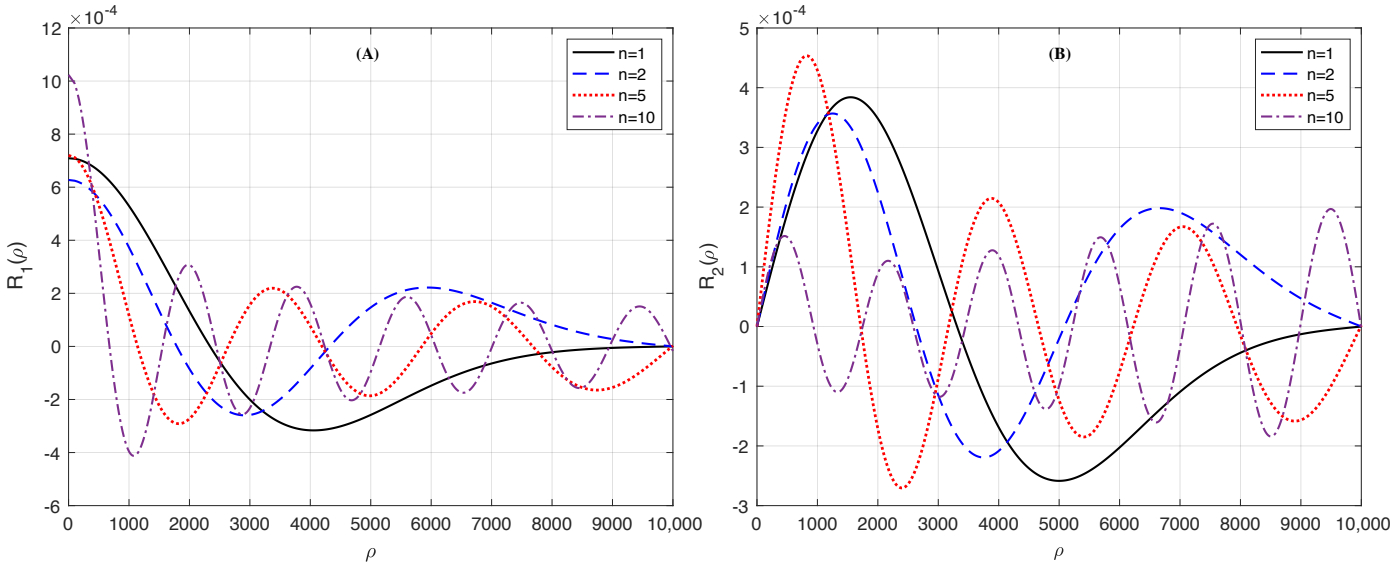

Figure 2. Wave functions for $B = 5 \times 10^{-5}$ au, versus the radius ρ (in au) with $m = 0$ and different values of of n for (**A**) spin up and (**B**) spin down. n gives the number of nodes of the wave function. The presence of nodes in the wave function decreases the area of disk where it is possible to find the charge: because of the uncertainty relation the overal effect is to increase the energy of the states with n.

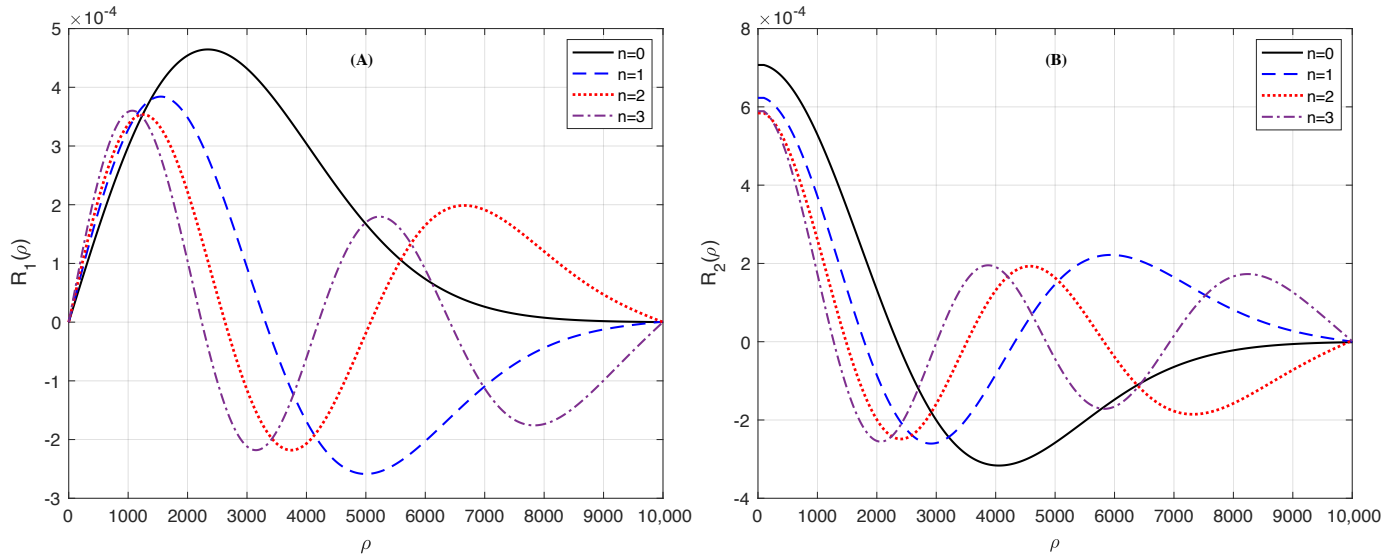

Figure 3. Wave functions for $B = 5 \times 10^{-5}$ au versus the radius ρ (in au) with $m = -1$ and different values of n for (**A**) spin up with n number of nodes and (**B**) for spin down with $n + 1$ number of nodes.

Figure 2 suggests a possibility of obtaining a spatial separation of the two-spin polarization. For example, for $m = 0$, the spin-up eigenstates, in Figure 2A, peak at the centre of the disk while the spin-down states, in Figure 2B, have a node at the same point. For the

case $m = -1$, shown in Figure 3, the situation is reversed and the spin-down states peak at the centre. However, to stress is that the relevant quantity is $|R_k(\rho)|^2\rho$, (see Equation (43)), which emphasizes the mid to the detriment of the innermost (where $\rho = 0$) and peripheral (where $R_k(\rho) = 0$) parts of the disk. For example, in Figure 4, we show $|R_k(\rho)|^2\rho$ ($k = 1, 2$) for $B = 5 \times 10^{-5}$ au, $m = 0$ and $n = 1$ whose relative eigenstates are shown in Figure 2. However, still from Figure 4, one can see that a certain amount of external control for the location of the peak of the two-spin polarization is possible by using the quantum numbers n and m as knobs.

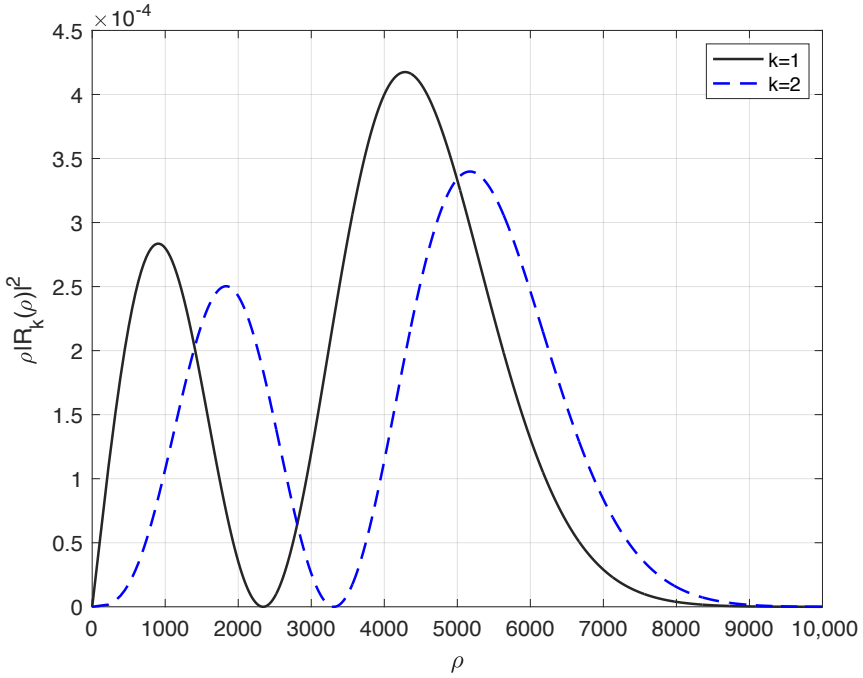

Figure 4. Probability density, $w(\rho) = \rho|R_k(\rho)|^2$, versus the radius ρ (in au) with $k = [1, 2]$, for the spin up and down states. $w(\rho)d\rho$ gives the probability of finding the particle in the infinitesimal annulus $[\rho, \rho + d\rho]$. The magnetic field is $B = 5 \times 10^{-5}$ au, $m = 0$ and $n = 1$. To be compared with Figure 2 where the eigenstates are plotted. $w(\rho)$ for the two considered states peaks at different locations; the disk presents, therefore, concentric regions of different spin polarisation.

In Figure 5, we show the eigenstates of the Dirac electron versus ρ for $B_0 = 5.0 \times 10^{-5}$ au and for several values of the orbital angular momentum $m \geq 0$ for both the cases with spin up and down. In all the curves, $n = 0$ and thus the wave function shows no nodes. A few interesting features emerge. As to be expected, states with a quite large value of the orbital angular momentum are pushed toward the outer region of the disk as if a centrifugal force is acting on the particle even if it is massless. Recently the study of trapped Bose–Einstein condensates (BEC) led to the discussion of quantised vortices [32] which generally can be defined as states possessing a well-defined orbital quantum number, μ. Such states and their control to design devices for reading and writing in computers are today an extensive research activity [38]. Actually, the possibility of stacking or arranging rings and disks in a coplanar geometry to let them communicate via their magnetic field is appealing [39]; from this point of view, the use of graphene annuli and disks is particularly attractive because modern technology permits the preparation of multi-layered graphene sheets.

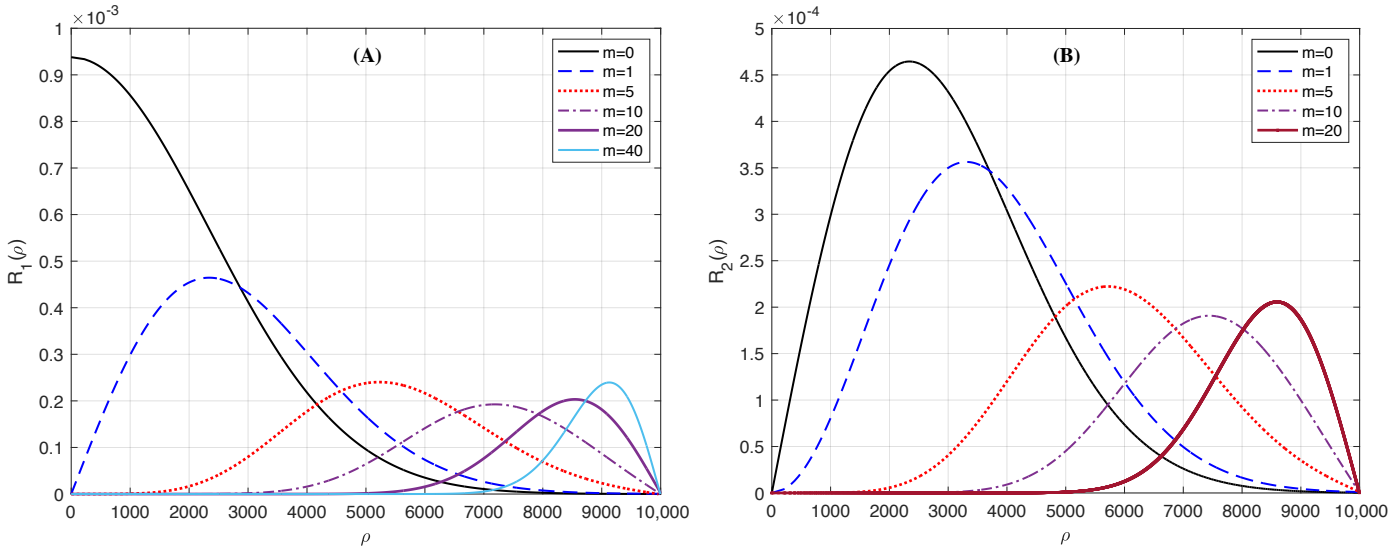

Figure 5. Wave function versus ρ (in au) for $B_0 = 5 \times 10^{-5}$ au, $n = 0$, and different values of m for (**A**) spin up and (**B**) spin down. Both spin case show the same behaviour: the peak of the wave functions shifts towards the edge of the disk when m increases. This feature is expected: a quite large angular momentum is obained when the particle orbits at relatively large distance from the centre.

One can associate these concept of energetically rotating states possessing a relatively large orbital angular momentum to a vortex. In relativistic quantum theory for a free particle, the orbital $\vec{L}$ and the spin $\vec{\sigma}$ angular momenta are not individually constant, so we are led to interpret the state ψ_3 as a vortex having j_3 vorticity *number*. Moreover, states with large and small enough values of m overlap quite little and a way to associate different bits of information to them should be envisaged.

Figure 6 clarifies the role of the nodes of the eigenstates for negative m with the curves taken for $m = -2$ and the states have different number of nodes in spite of their same energy. Summarizing, for $m \geq 0$, the degenerate eigenstates can be labelled by the two quantum numbers, m and n, with n counting the number of nodes of the eigenstates; for $m < 0$, on the other hand, n can only set the order of the states.

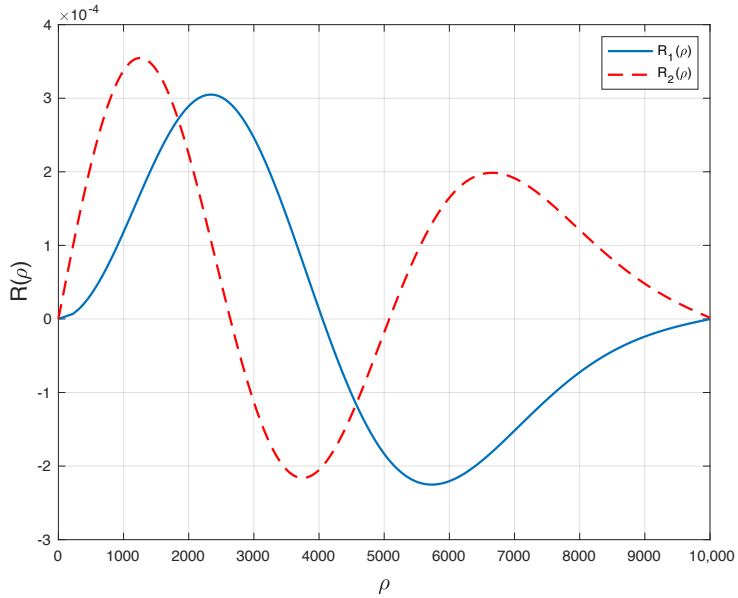

Figure 6. Eigenstates versus the radius ρ (in au) for $m = -2$ and $B_0 = 5 \times 10^{-5}$ au for the states having the same energy, $E/u_F = 8.3 \times 10^2$ au, but different number of nodes.

In Section 1, we mentioned the difficulty, encountered in relativistic quantum theory, of confining electrons by means of a potential barrier.

This difficulty arises from the point that the negative energy states see the barrier as a well and are, then, pulled to climb the cliff. In graphene, the Klein paradox is present but appears as a transition between conduction and valence band of the lattice; however, confinement can be obtained by means of a magnetic field. The curves in Figure 7 show few states for $n = m = 0$ and spin up, for sake of simplicity. It is clear enough that the magnetic field has a relevant importance in confining the charges; In general, for a relatively large magnetic field, the wave function does not approach the edge of the disk. Here, one can see how the Klein paradox may be controlled. The paradox lies on the basis that a positive energy solution of the Dirac equation (the electron in the conduction band) cannot be confined by a repulsive potential since in reaching the potential it makes a transition toward a negative energy solution (the electron in the valence band). However, the magnetic field forbids the approach of the particle to the border of the disk and the consequent interaction with the potential; we consider this one of the relevant results of this paper. It is essentially to stress that the necessary magnetic field is rather large but the physical situation is not ordinary in describing massless charges; the use of a smaller disk is even detrimental for the confinement as a larger field is required. Actually, the energy of the electrons increases by decreasing the radius ρ_1 and this outcome can be exploited if wanted. As a side effect, it can be noticed that a stretching force is exerted by the charge on the disk [36] wich increases with the confinement and, consequently, with the magnetic field. Such a stretching may become detectable in the near future.

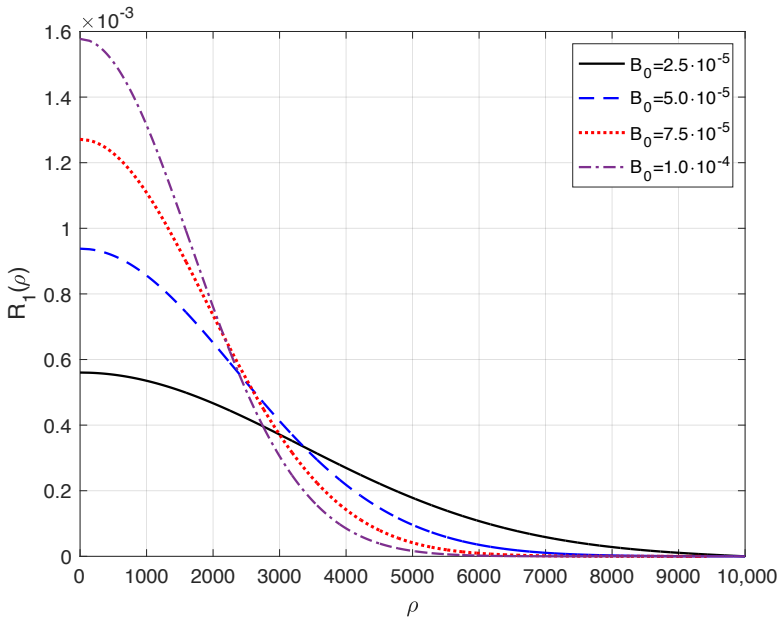

Figure 7. Sequence of four eigenstates of the disk versus the radius ρ (in au) for $m = n = 0$ and different magnetic field intensity, B_0. The plots well demonstrate the confining action of the magnetic field. The field $B_0 = 2.5 \cdot 10^{-5}$ au has indeed a relatively low confining property while the field $B_0 = 10^{-4}$ au confines the charge within the origin and $\rho \cong 2500\ a_0$. The use of a smaller disk would require a stronger field for efficient confinement.

In conclusion, in this paper, we study the wave function of the charge carriers in a considerably large disk of graphene in the presence of a static magnetic field orthogonal to the plane of the disk. Thanks to the particular symmetry of the lattice, the valence electrons of the carbon atoms can be treated as having null mass, like the photon, but moving with a speed much slower that the average speed of the electron in the hydrogen ground state. In spite of this observation, because of the massless condition, the charges can be described only by means of the relativistic Dirac theory with its intrinsic positive–negative energy

dualism. Thus, the graphene provides a handy way to observe massless particles that can be acted upon by electromagnetic fields.

The analysis shows that the magnetic field acts as a confining tool of the charges and, perhaps, it may provide the only confinement parameter to defeat the Klein paradox. The eigenstates and related energy can be labelled by the integer quantum numbers m and n. The key result is that the position of the peak of the eigenstates can be manipulated using the quantum numbers m and n as control knobs and can be made to range from the inner to the outer part of the disk. In this way, by linear superposition it is possible, in a graphene disk, to construct states with different peaks. By associating a bit of information to any eigenstate of the superposition, it is possible to store many bits of information in the disk. Moreover, the disk can support states with high values of the orbital angular momentum m, thus providing a way to observe states with large enough vortex charge. In this perspective, annuli and disks of graphene have been extensively studied both from the analytical and the fully numerical point of view to investigate their use as quantum dots by varying the edge confinement potential [12,13,15,40].

Recapitulating, in this paper, we obtained the wave function of the states of the electrons in a magnetised disk of graphene in strict analytical form both for the up and down spin components and labelled them according to two quantum numbers for the orbital angular momentum and for the nodes of the wave functions. These quantum numbers can be used as a knobs for controlling the position of the peaks of the states in the disk in the context of storing bits of information. We showed that the system can support states with quite large angular momentum and suggested that the relativistic treatment does not permit the definition of vortex states as endowed with a precise orbital angular momentum. However, the total angular momentum is a proper quantum number and allows a redefinition of the vortex state. A key new contribution is the evaluation of the states for several values of the magnetic field and proved that confinement may be achieved by means of a magetic field. All of these characteristics make the graphene fragments a quite particular object for basic and applicative research.

Author Contributions: Conceptualization, E.F.; methodology, D.C., P.P.C. and E.F.; software, D.C., P.P.C. and E.F.; validation, D.C. and P.P.C.; formal analysis, E.F.; writing—original draft preparation, E.F.; writing—review and editing, D.C., P.P.C. and E.F. All authors have read and agreed to the published version of the manuscript.

Funding: This research received no external funding.

Data Availability Statement: The data presented in this study are available on request from the corresponding author.

Conflicts of Interest: The authors declare no conflict of interest.

Appendix A. The Spin-Down Solution

In this Appendix, details of the determination of the radial line of the spin-down wave function $R_2(\rho)$ are given. Once that the expression for the spin up $R_1(\rho)$ has been derived, from the second part of Equation (16), one can see that $R_2(\rho)$ can be obtained through the derivative of the spin-up wave function $R_1(\rho)$ that is the linear combination of the two CHFs as given in Equations (29) and (30).

According to Equations (13.4.8) and (13.4.21) of ref. [41], the derivatives of the two independent CHFs are

$$M'(a,b,z) = \frac{a}{b} M(a+1.b+1,z); \quad U'(a,b,z) = -aU(a+1,b+1,z), \tag{A1}$$

where the prime denotes derivative with respect to z. Thus, the following two involved expression are derived:

$$\begin{aligned}\frac{d}{d\rho}R_{1;1}(\rho) &= \mathrm{e}^{-\frac{\rho^2}{2\lambda^2}}\left[\left(-\frac{\rho}{\lambda^2}\left(\frac{\rho}{\lambda}\right)^{|m|}+|m|\frac{\rho^{|m|-1}}{\lambda^{|m|}}\right)M\left(a,b,\frac{\rho^2}{\lambda^2}\right)\right.\\ &+ \left.\left(\frac{\rho}{\lambda}\right)^{|m|}\frac{a}{b}\frac{2\rho}{\lambda^2}M\left(a+1,b+1,\frac{\rho^2}{\lambda^2}\right)\right]\\ &= \mathrm{e}^{-\frac{\rho^2}{2\lambda^2}}\frac{\rho^{|m|-1}}{\lambda^{|m|}}\left[\left(-\frac{\rho^2}{\lambda^2}+|m|\right)M\left(a,b,\frac{\rho^2}{\lambda^2}\right)\right.\\ &+ \left.\frac{a}{b}\frac{2\rho^2}{\lambda^2}M\left(a+1,b+1,\frac{\rho^2}{\lambda^2}\right)\right] \qquad \text{(A2)}\end{aligned}$$

and

$$\begin{aligned}\frac{d}{d\rho}R_{1;2}(\rho) &= \mathrm{e}^{-\frac{\rho^2}{2\lambda^2}}\left[\left(-\frac{\rho}{\lambda^2}\left(\frac{\rho}{\lambda}\right)^{|m|}+|m|\frac{\rho^{|m|-1}}{\lambda^{|m|}}\right)U\left(a,b,\frac{\rho^2}{\lambda^2}\right)\right.\\ &- \left.\left(\frac{\rho}{\lambda}\right)^{|m|}a\frac{2\rho}{\lambda^2}U\left(a+1,b+1,\frac{\rho^2}{\lambda^2}\right)\right]\\ &= \mathrm{e}^{-\frac{\rho^2}{2\lambda^2}}\frac{\rho^{|m|-1}}{\lambda^{|m|}}\left[\left(-\frac{\rho^2}{\lambda^2}+|m|\right)U\left(a,b,\frac{\rho^2}{\lambda^2}\right)\right.\\ &- \left.a\frac{2\rho^2}{\lambda^2}U\left(a+1,b+1,\frac{\rho^2}{\lambda^2}\right)\right]. \qquad \text{(A3)}\end{aligned}$$

The expression for $R_{2;1}$ can be obtained from

$$\begin{aligned}\mathcal{A}_{2;1} &\equiv \left[\hbar c\left(\frac{d}{d\rho}-\frac{m}{\rho}\right)+\frac{qB_0}{2}\rho\right]R_{1;1}\\ &= \hbar c\mathrm{e}^{-\frac{\rho^2}{2\lambda^2}}\frac{\rho^{|m|-1}}{\lambda^{|m|}}\left[\left(-\frac{\rho^2}{\lambda^2}+|m|\right)M\left(a,b,\frac{\rho^2}{\lambda^2}\right)\right.\\ &+ \left.2\frac{a}{b}\frac{\rho^2}{\lambda^2}M\left(a+1,b+1,\frac{\rho^2}{\lambda^2}\right)\right]\\ &- \hbar cm\mathrm{e}^{-\frac{\rho^2}{2\lambda^2}}\frac{\rho^{|m|-1}}{\lambda^{|m|}}M\left(a,b,\frac{\rho^2}{\lambda^2}\right)+\frac{qB_0}{2}\rho\mathrm{e}^{-\frac{\rho^2}{2\lambda^2}}\left(\frac{\rho}{\lambda}\right)^{|m|}M\left(a,b,\frac{\rho^2}{\lambda^2}\right)\\ &= \mathrm{e}^{-\frac{\rho^2}{2\lambda^2}}\frac{\rho^{|m|-1}}{\lambda^{|m|}}\left\{\left[\hbar c\left(-\frac{\rho^2}{\lambda^2}+|m|-m+\frac{qB_0}{2\hbar c}\rho^2\right)\right]M\left(a,b,\frac{\rho^2}{\lambda^2}\right)\right.\\ &+ \left.2\frac{a}{b}\frac{\rho^2}{\lambda^2}M\left(a+1,b+1,\frac{\rho^2}{\lambda^2}\right)\right\} \qquad \text{(A4)}\end{aligned}$$

and, with

$$\frac{qB_0}{2\hbar c}=\eta\frac{|q|B_0}{2\hbar c}=\frac{\eta}{\lambda^2}\,, \qquad \text{(A5)}$$

$$\begin{aligned}\mathcal{A}_{2;1} = \mathrm{e}^{-\frac{\rho^2}{2\lambda^2}}\frac{\rho^{|m|-1}}{\lambda^{|m|}}&\left\{\left[\hbar c\left((\eta-1)\frac{\rho^2}{\lambda^2}+|m|-m\right)\right]M\left(a,b,\frac{\rho^2}{\lambda^2}\right)\right.\\ &\left.+\,2\frac{a}{b}\frac{\rho^2}{\lambda^2}M\left(a+1,b+1,\frac{\rho^2}{\lambda^2}\right)\right\}. \qquad \text{(A6)}\end{aligned}$$

Similar algebra lead to the expression for $R_{2;2}$.

References

1. Neto, A.H.C.; Guinea, F.; Peres, N.M.R.; Novoselov, K.S.; Geim, A.K. The electronic properties of graphene. *Rev. Mod. Phys.* **2009**, *81*, 109–162. [CrossRef]
2. Wang, D.; Jin, G. Magnetically confined states of Dirac electrons in a graphene-based quantum annulus. *Europhys. Lett.* **2009**, *88*, 17011. [CrossRef]

3. Katsnelson, M.I.; Novoselov, K.S.; Geim, A.K. Chiral tunnelling and the Klein paradox in graphene. *Nat. Phys.* **2006**, *2*, 620–625. [CrossRef]
4. Goerbig, M.O. Electronic properties of graphene in a strong magnetic field. *Rev. Mod. Phys.* **2011**, *83*, 1193–1243. [CrossRef]
5. Sakurai, J.J. *Advanced Quantum Mechanics*; Addison-Wesley Publishing Company: Boston, MA, USA, 1967. Available online: https://archive.org/details/advanced-quantum-mechanics-by-j.-j.-sakurai-z-lib.org (accessed on 15 January 2024).
6. Allain, P.E.; Fuchs, J.N. Klein tunneling in graphene: Optics with massless electrons. *Eur. Phys. J. B* **2011**, *83*, 301. [CrossRef]
7. Jin, G.; Wang, D. Bound states of Dirac electrons in a graphene-based magnetic quantum dot. *Phys. Lett. A* **2009**, *373*, 4082–4085. [CrossRef]
8. Liu, S.; Nurbawono, A.; Guo, N.; Zhang, C. Massless Dirac fermions in graphene under an external periodic magnetic field. *J. Phys. Cond. Mat.* **2013**, *25*, 395302. [CrossRef]
9. Downing, C.A.; Pearce, A.R.; Churchill, R.J.; Portnoi, M.E. Optimal traps in graphene. *Phys. Rev. B* **2015**, *92*, 165401. [CrossRef]
10. Downing, C.A.; Portnoi, M.E. Massless dirac fermions in two dimensions: Confinement in nonuniform magnetic fields. *Phys. Rev. B* **2016**, *94*, 165407. [CrossRef]
11. Eshghi, M.; Mehraban, H.; Azar, I.A. Eigenspectra and wave functions of the massless Dirac fermions under the nonuniform magnetic fields in graphene. *Physica E* **2017**, *94*, 106–112. [CrossRef]
12. Hewageegana, P.; Apalkov, V. Electron localization in graphene quantum dots. *Phys. Rev. B* **2008**, *77*, 245426. [CrossRef]
13. Maksym, P.A.; Roy, M.; Craciun, M.F.; Russo, S.; Yamamoto, M.; Tarucha, S.; Aoki, H. Proposal for a magnetic field induced graphene dot. *J. Phys. Conf. Ser.* **2010**, *245*, 012030. [CrossRef]
14. Freitag, N.M.; Chizhova, L.A.; Nemes-Incze, P.; Woods, C.R.; Gorbachev, R.V.; Cao, Y.; Geim, A.K.; Novoselov, K.S.; Burgdörfer, J.; Libisch, F.; et al. Electrostatically confined monolayer graphene quantum dots with orbital and valley splittings. *Nano Lett.* **2016**, *16*, 5798–5805. [CrossRef]
15. Grushevskaya, V.; Krylov, G.G.; Kruchinin, S.P.; Vlahovic, B.; Bellucci, S. Electronic properties and quasi-zero-energy states of graphene quantum dots. *Phys. Rev. B* **2021**, *103*, 235102. [CrossRef]
16. Zasada, I.; Cerdá, J.I.; Ślot, M. Realistic systems testing Klein tunneling in graphene: An ab initio calculations. *Physica B* **2023**, *668*, 415213. [CrossRef]
17. Lee, C.; Wei, X.; Kysar, J.W.; Hone, J. Measurement of the elastic properties and intrinsic strength of monolayer graphene. *Science* **2008**, *321*, 385–388. [CrossRef]
18. Novoselov, K.S.; Geim, A.K.; Morozov, S.V.; Jiang, D.; Zhang, Y.; Dubonos, S.V.; Grigorieva, V.; Firsov, A.A. Electric field effect in atomically thin carbon films. *Science* **2004**, *306*, 666–669. [CrossRef]
19. Miao, X.; Tongay, S.; Petterson, M.K.; Berke, K.; Rinzler, A.G.; Appleton, B.R.; Hebard, A.F. High efficiency graphene solar cells by chemical doping. *Nano Lett.* **2012**, *12*, 2745–2750. [CrossRef]
20. Ganeev, R.A.; Suzuki, M.; Baba, M.; Yoneya, S.; Kuroda, H. Graphene-containing plasma: A medium for the coherent extreme ultraviolet light generation. *JETP Lett.* **2014**, *100*, 434–438. [CrossRef]
21. Yoshikawa, N.; Tamaya, T.; Tanaka, K. High-harmonic generation in graphene enhanced by elliptically polarized light excitation. *Science* **2017**, *356*, 736–738. [CrossRef]
22. Ganeev, R.A. *Plasma Harmonics*; Jenny Stanford Publishing/Taylor & Francis Group: New York, NY, USA, 2014. . [CrossRef]
23. Chen, H.; Zhang, X.-L.; Zhang, Y.-Y.; Wang, D.; Bao, D.-L.; Que, Y.; Xiao, W.; Du, S.; Ouyang, M.; Pantelides, S.T.; et al. Atomically precise, custom-design origami graphene nanostructures. *Science* **2019**, *365*, 1036–1040. [CrossRef]
24. Ho, D.T.; Ho, V.H.; Babar, V.; Kim, S.Y.; Schwingenschlögl, U. Complex three-dimensional graphene structures driven by surface functionalization. *Nanoscale* **2020**, *12*, 10172. [CrossRef]
25. Cai, J.; Estakhrianhaghighi, E.; Akbarzadeh, A. Functionalized graphene origami metamaterials with tunable thermal conductivity. *Carbon* **2022**, *191*, 610–624. [CrossRef]
26. Cricchio, D.; Fiordilino, E. Dynamic clock generator and memory mass device using a quantum ring driven by three-color laser fields. *RSC Adv.* **2021**, *11*, 26168. [CrossRef]
27. Zhou, X.; Tartakovskaya, E.V.; Kakazei, G.N.; Adeyeye, A.O. Engineering spin wave spectra in thick $Ni_{80}Fe_{20}$ rings by using competition between exchange and dipolar fields. *Phys. Rev. B* **2021**, *104*, 214402. [CrossRef]
28. Zhitlukhina, E.; Belogolovskii, M.; Seidel, P. Microwave-driven persistent currents in a nanoscale quantum ring. *Appl. Nanosci.* **2022**, *12*, 377–383. [CrossRef]
29. Motlagh, A.T.; Salehani, H.K. Design and simulation of a binary full adder based on quantum rings. *Physica E* **2022**, *142*, 115232. [CrossRef]
30. He, Y.; Guo, H.; Chien, C.-C. BCS-BEC crossover of atomic Fermi superfluid in a spherical bubble trap. *Phys. Rev. A* **2022**, *105*, 033324. [CrossRef]
31. Lado, J.L.; García-Martínez, N.; Fernández-Rossier, J. Edge states in graphene-like systems. *Synth. Met.* **2015**, *210*, 56–67. [CrossRef]
32. Fetter, A.L.; Svidzinsky, A.A. Vortices in a trapped dilute Bose–Einstein condensate. *J. Phys. Condens. Matt.* **2001**, *13*, R135–R194. [CrossRef]
33. Andriati, A.; Brito, L.; Tomio, L.; Gammal, A. Stability of a Bose-condensed mixture on a bubble trap. *Phys. Rev. A* **2021**, *104*, 033318. [CrossRef]

34. Bereta, S.J.; Caracanhas, M.A.; Fetter, A.L. Superfluid vortex dynamics on a spherical film. *Phys. Rev. A* **2021**, *103*, 053306. [CrossRef]
35. Padavić, K.; Sun, K.; Lannert, C.; Vishveshwara, S. Vortex-antivortex physics in shell-shaped Bose-Einstein condensates. *Phys. Rev. A* **2020**, *102*, 043305. [CrossRef]
36. Fiordilino, E. Laser assisted Dirac electron in a magnetized annulus. *Symmetry* **2021**, *13*, 642. [CrossRef]
37. Riley, K.F.; Hobson, M.P.; Bence, S.J. *Mathematical Methods for Physics and Engineering;* Cambridge University Press : Cambridge, UK, 2006. [CrossRef]
38. Kläui, M.; Rothman, J.; Lopez-Diaz, L.; Vaz, C.A.F.; Bland, J.A.C.; Cui, Z. Vortex circulation control in mesoscopic ring magnets. *Appl. Phys. Lett.* **2001**, *78*, 3268–3270. [CrossRef]
39. Nam, C.; Mascaro, M.D.; Ross, C.A. Magnetostatic control of vortex chirality in Co thin film rings. *Appl. Phys. Lett.* **2010**, *97*, 012505. [CrossRef]
40. Li, X.; Tao, L.; Chen, Z.; Fang, H.; Li, X.; Wang, X.; Xu, J.-B.; Zhu, H. Graphene and related two-dimensional materials: Structure-property relationships for electronics and optoelectronics. *App. Phys. Rev.* **2017**, *4*, 021306. [CrossRef]
41. Abramowitz, M.; Stegun, I.A. (Eds.) *Handbook of Mathematical Functions with Formulas, Graphs, and Mathematical Tables*; Dover Publications, Inc.: New York, NY, USA, 1972. Available online: https://archive.org/details/handbookofmathe000abra/ (accessed on 15 January 2024).